

Accepted Article

Title: Electronic State Manipulation of Surface Titanium Activates Dephosphorylation over TiO₂ Near Room Temperature

Authors: Quan Wang, Xianfeng Yi, Yu-Cheng Chen, Yao Xiao, Anmin Zheng, Jian Lin Chen, and Yung-Kang Peng

This manuscript has been accepted after peer review and appears as an Accepted Article online prior to editing, proofing, and formal publication of the final Version of Record (VoR). This work is currently citable by using the Digital Object Identifier (DOI) given below. The VoR will be published online in Early View as soon as possible and may be different to this Accepted Article as a result of editing. Readers should obtain the VoR from the journal website shown below when it is published to ensure accuracy of information. The authors are responsible for the content of this Accepted Article.

To be cited as: *Angew. Chem. Int. Ed.* 10.1002/anie.202104397

Link to VoR: <https://doi.org/10.1002/anie.202104397>

Electronic State Manipulation of Surface Titanium Activates Dephosphorylation over TiO₂ Near Room Temperature

Quan Wang,^[a] Xianfeng Yi,^[b] Yu-Cheng Chen,^[c] Yao Xiao,^[b] Anmin Zheng,^{*,[b]} Jian Lin Chen^[d] and Yung-Kang Peng^{*,[a,e]}

[a] Quan Wang, Prof. Yung-Kang Peng
Department of Chemistry, City University of Hong Kong, Hong Kong SAR.
E-mail: ykpeng@cityu.edu.hk

[b] Dr. Xianfeng Yi, Yao Xiao, Prof. Anmin Zheng
State Key Laboratory of Magnetic Resonance and Atomic and Molecular Physics, National Center for Magnetic Resonance in Wuhan, Key Laboratory of Magnetic Resonance in Biological Systems, Wuhan Institute of Physics and Mathematics, Innovation Academy for Precision Measurement Science and Technology, Chinese Academy of Sciences, Wuhan 430071, China.
E-mail: zhenganm@wipm.ac.cn

[c] Yu-Cheng Chen
Department of Mechanical Engineering, City University of Hong Kong, Hong Kong SAR, China.

[d] Prof. Jian Lin Chen
Department of Science, School of Science and Technology, The Open University of Hong Kong, Hong Kong SAR, China.

[e] Prof. Yung-Kang Peng
City University of Hong Kong Shenzhen Research Institute, Shenzhen 518057, China.

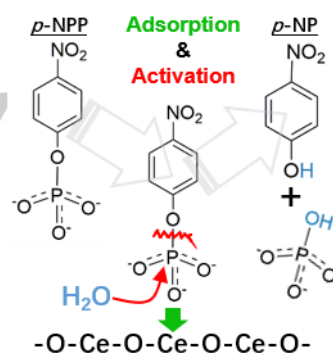
Supporting information for this article is given via a link at the end of the document.

Abstract: Dephosphorylation that removes a phosphate group from substrates is an important reaction for not only living organisms but also environmental protection. Although CeO₂ has been shown to catalyze this reaction, as one of the rare earth elements, cerium is low in natural abundance and has a narrow global distribution (> 90% of these reserves are located within six countries). It is thus imperative to find another element/material with high worldwide abundance that can also efficiently extract the phosphate out of agricultural wastes for phosphorus recycle. Using para-nitrophenyl phosphate (*p*-NPP) as the model compound, we demonstrate herein that TiO₂ with F-modified (001) surface can activate *p*-NPP dephosphorylation at temperature as low as 40 °C. By probe-assisted nuclear magnetic resonance (NMR), it was revealed that the strong electron withdrawing effect of fluorine makes Ti atoms (i.e., the active sites) on (001) surface very acidic. The bidentate adsorption of *p*-NPP on this surface further promotes its subsequent activation with barrier ~20 kJ/mol lower than that of pristine (001) and (101) surfaces, allowing the activation of this reaction at nearly room temperature (from > 80 °C).

Introduction

Phosphorus is the crucial element in living organisms that involves many biologically important processes such as plant growth, energy storage, photosynthesis, cell regulation and signaling etc.^[1] Phosphatase, a natural enzyme widely found in living systems, can remove phosphate groups from organic substrates into inorganic phosphates and hence play a significant role in the recycle of phosphorus^[2]. The majority of the environmental phosphorus came from animal wastes before the 18th century. Nowadays, more than 80% phosphorus used in fertilizers relies on the non-renewable phosphate rocks^[3]. Given that the demand for phosphorus fertilizers continues to grow with population, the global reserve of phosphate rocks is estimated to be depleted within this century^[4]. However, it is not practical to use natural enzymes (i.e., phosphatase) for the recycle of environmental phosphorus since they suffer from easy denaturation and high costs in both preparation and purification.

It is thus imperative to develop robust catalysts that can extract the phosphorus out of phosphorylated wastes in an ecologically sustainable manner.



Scheme 1. Schematic illustration of catalytic *p*-NPP dephosphorylation over CeO₂.

Pioneered by Tan et al in 2008, CeO₂ nanoparticles (NPs) were adopted to mimic phosphatases catalyzing the dephosphorylation of various phosphopeptides^[5]. The phosphatase-like activity of CeO₂ NPs was attributed to the activation of targets' phosphoryl oxygen by surface Ce for later S_N2 hydrolysis (Scheme 1). The phosphate anions can thus be extracted from animal/agriculture wastes and recycled for further applications to achieve phosphorus sustainability^[1-4]. Using para-nitrophenyl phosphate (*p*-NPP) as a model molecule, Tan et al.^[5] firstly suggested a surface Ce⁴⁺-mediated pathway while later Kuchma et al.^[6] found the activity is proportional to the concentration of surface Ce³⁺. A balanced surface Ce⁴⁺/Ce³⁺ ratio^[7] and surface oxygen vacancy^[8] were also proposed the key factor facilitating this CeO₂-catalyzed dephosphorylation. Although a wide range of Ce-based catalysts have been reported to catalyze this reaction^[9-12], the key surface Ce species and the underlying mechanism are still unclear. Using probe-assisted nuclear magnetic resonance (NMR), we recently demonstrated that the electronic state (i.e., Lewis acidity) of surface Ce shifts "continuously" with its local structure and cannot be ascribed to the "discrete" oxidation state (e.g., 3+ and

4+ for Ce) as in literatures above^[13]. The surface Ce with strong Lewis acidity was found to facilitate not only the adsorption of *p*-NPP but also its subsequent activation.

Although cerium is the most abundant rare earth element, it comprises only 0.0046 wt% of the Earth's crust. Most importantly, the global distribution of rare earth elements is extremely heterogeneous. According to estimates by the U.S. Geological Survey, more than 90% of these reserves are located within six countries: China (36.6%), Brazil (18.3%), Vietnam (18.3%), Russia (10%), India (5.75%) and Australia (2.75%)^[14]. From sustainable point of view, it is crucial to find another element with high worldwide abundance that can also extract the phosphate out of agricultural wastes for phosphorus recycle. Titanium is the ninth abundant element comprising about 0.565 wt% of the Earth's crust (i.e., more than 100 times of cerium). It is much cheaper and can be found in nearly all rocks/sediments among the crusts of Earth. Over the past decades, its oxide form, TiO₂, has received a tremendous attention due to many important applications ranging from the conventional areas (e.g., paint, cosmetic, toothpaste, etc.) to the advanced photo-electro areas^[15]. The acid-base applications of TiO₂ NPs are equally important however less explored presumably due to the moderate Lewis acidity of surface Ti atoms among transition metal oxides.

Given that each terminal facet of a crystallite possesses distinct surface energy, the Lewis acidity of surface cations is believed to vary with host facets and hence influence the adsorption/activation of coming reactant^[15,16]. Surface pre-adsorbed species (e.g., surfactant) with different electronegativity can further modify this property on a given facet^[17]. Accordingly, we manipulate the electronic state of surface Ti in this study by tuning its local structure from anatase TiO₂(101) to TiO₂(001) with different surface adsorbed species (O, F). Fluorine was selected here as the only element more electronegative ($\chi = 3.98$) than oxygen ($\chi = 3.44$) in the periodic table. Interestingly, the activation energy for *p*-NPP dephosphorylation is considerably reduced for TiO₂ samples with F-modified (001) (i.e., F-(001)) surface. Probe-assisted NMR reveals that the Lewis acidity of Ti atoms on this surface is comparable to super solid acids and hence activates *p*-NPP dephosphorylation at temperature as low as 40 °C. Moreover, the reaction rate was found to only associate with the area of F-(001) surface for a given TiO₂ crystallite while the rest surfaces such as pristine (101) and (001) are both silent at temperature < 80 °C. In addition to NMR, techniques such as infrared (IR) and transmission electron microscopy-electron energy loss spectroscopy (STEM-EELS) were further adopted to unravel the adsorption and activation structures of *p*-NPP on this particular F-(001) surface.

Results and Discussion

Although anatase TiO₂ are often covered with thermodynamically stable (101) facet (0.44 J m⁻²) in nature, Yang et al. (2008) found that fluorine can specifically bind/stabilize the high-energy (001) facet (0.90 J m⁻²) and hence reverse the relative thermodynamic stability of these two facets^[18]. Since then, anatase TiO₂ with different ratio of (001)

and (101) terminal facets have been prepared by varying the amount of HF added during hydrothermal synthesis for the study of facet activity in a wide range of applications^[19, 20]. The extra addition of alcohols was recently found can not only make them well-defined but also fine-tune the (001)/(101) ratio by affecting the hydrolysis-condensation rate of titanium(IV) butoxide^[21-24].

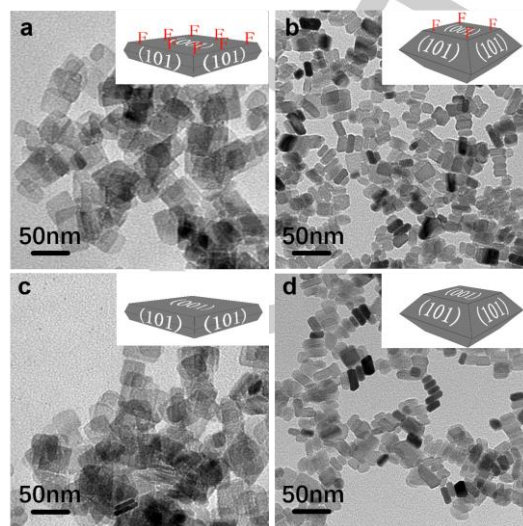


Figure 1. TEM images of TiO₂ (a) F-NS-1, (b) F-NS-10, (c) and (d) are their F removed samples denoted as NS-1 and NS-10.

Herein, TiO₂ samples with different (001)/(101) ratio were prepared with a fixed amount of HF (i.e., 0.8 mL) in the presence of 1 mL (denoted as F-NS-1) and 10 mL (denoted as F-NS-10) methanol (see experimental section for details). F-NS-1 (Figure 1a) and F-NS-10 (Figure 1b) indeed reveal different morphologies as evidenced by their corresponding TEM images. The anatase structure of both samples was confirmed by X-ray diffraction (XRD) analysis in Figure S1. This result can also be supported by the lattice spacings of 0.235 nm found in these two samples (Figure S2), corresponding to the (001) crystallographic plane of anatase TiO₂. The percentage of (001) and (101) facet exposed in both samples was further estimated by the Wulff construction model (Figure S3)^[25, 26]. As summarized in Table S1, more than 70 % of F-NS-1 surface is enclosed by (001) facet while F-NS-10 preferentially exposes (101) facet (i.e., 64.7 %). Note in this table that the percentage of the dominant facet for each sample is more than doubled than the minor facet of the other sample. Although the same amount of HF was used for their preparation (i.e., 0.8 mL), the resulting fluorine concentration is believed proportional to the area of their (001) surface. Indeed, F-NS-1 with dominant (001) surface shows a stronger F signal than F-NS-10 in the corresponding X-ray photoelectron spectroscopy (XPS) F_{1s} spectra (Figure S4). NaOH wash was used herein to remove F from the (001) surface of both samples (denoted as NS-1 and NS-10) as often adopted in literatures^[19, 20, 27, 28]. This post-treatment is very effective on F removal that no apparent XPS F_{1s} signal can be observed for NS-1 and NS-10 (Figure S4) while keeping their morphology (Figure 1c,d), crystallinity (Figure S1), Raman structural fingerprint (Figure S5) and surface area (Figure S6 and Table S1) nearly unchanged.

The dephosphorylation activity of F-NS-1, F-NS-10 and their F removed samples (i.e., NS-1 and NS-10) was evaluated

using *para*-nitrophenyl phosphate (*p*-NPP) as a model molecule^[5-8,13]. Since the characteristic absorption peaks of *p*-NPP (313 nm) and its hydrolyzed form *para*-nitrophenol (*p*-NP, 405 nm) are well-separated, the progress of dephosphorylation can thus be tracked by UV-vis spectroscopy. Figure 2a shows the time-dependent UV-vis spectra of *p*-NPP dephosphorylation collected over F-NS-1 at 60 °C. As the reaction proceeds, the signal of *p*-NP at 403 nm enhances pronouncedly at the cost of *p*-NPP at 313 nm due to the difference in their absorption coefficient. Since the adsorption of *p*-NPP varies a lot between TiO₂ samples (vide infra) while the product (i.e., *p*-NP) desorbs easily from their surfaces (by water solvation), the generation of *p*-NP is thus used for activity comparison and later kinetic study at different temperatures. The yield of *p*-NP can be obtained by a calibration plot with a series of *p*-NP solutions with known concentration (Figure S7). As shown in Figure 2b, F-NS-1 provides the highest activity followed by F-NS-10 with the yield of *p*-NP as 39.03% and 28.30% by 6 hours at 60 °C. While for the F removed samples (i.e., NS-1 and NS-10) their *p*-NP yield maintains at around 5% at this temperature and below (Figure S8a,b). Note that the amount of *p*-NP produced also decreases the pH of the solution as reaction proceeds (see Figure S9 for detail). To test whether fluoride alone or fluoride with clean TiO₂ can trigger the dephosphorylation of *p*-NPP, two sets of control experiments were conducted with reaction solutions containing (1) NaF (13.86 mg) alone and (2) NaF (13.86 mg) and NS-1 (6 mg). The amount of NaF added here was determined by the concentration of HF used in the synthesis of F-NS-1. As shown in Figure S10, the introduction of fluoride has a very minor effect on the dephosphorylation of *p*-NPP compared to that of blank. This can also be evidenced by the tiny change of *p*-NP yield after adding NaF to solution containing NS-1. Since no leakage of fluorine was detected by ¹⁹F NMR during the cyclic catalytic testing of F-NS-1 (see Figure S11 for detail), the high *k* constant obtained for this sample (also for F-NS-10) in Figure 2c thus suggests that the activation of *p*-NPP over Ti atoms is due to the presence of surface attached fluorine.

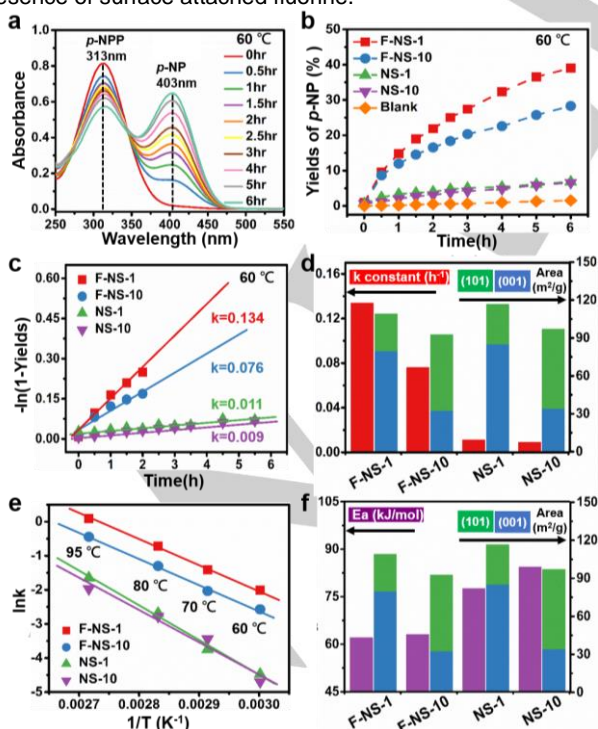


Figure 2. (a) The UV-vis spectra collected for the F-NS-1 sample at 60 °C as a function of time. (b) The time-dependent *p*-NP yield (defined as C_t/C_0 , where C_t refers concentration of *p*-NP at a given time, and C_0 refers to initial *p*-NPP concentration) of TiO₂ samples at 60 °C and (c) the corresponding kinetics analysis. (d) Comparison of *k* constant obtained at 60 °C and (101)/(001) surface area among TiO₂ samples. (e) Arrhenius plots for the activation energy of TiO₂ samples and (f) the comparison with their corresponding (101)/(001) surface area.

Since those Ti atoms are hosted by various surfaces, the obtained *k* constant was further compared with the facet distribution for a given TiO₂ sample to identify their location (Figure 2d). As expected, the *k* constant for the as-prepared TiO₂ samples (i.e., F-NS-1 and F-NS-10) was found proportional to the area of F-(001) surface while no such correlation can be observed for F removed samples (i.e., NS-1 and NS-10). For example, the F-NS-1 with doubled area of F-(001) surface (cf. F-NS-10, Table S1) provides *k* constant nearly two times higher than that of F-NS-10 at 60 °C (Figure 2c). In fact, the F-(001) surface of a given TiO₂ sample can activate this reaction at temperature as low as 40 °C (Figure S8b), which is in stark contrast to pristine (001) and rest (101) surfaces catalyzing this reaction at temperature higher than 80 °C (Figure S8e,f). This can also be evidenced by their *k* constant in Table S2 since the rate of an activated reaction should in theory double for every 10 °C rise in temperature. Note that this reaction without catalyst becomes active at 95 °C with activity even comparable to clean TiO₂ samples (i.e., NS-1 and NS-10, Figure S8f). The *k* constant of F-NS-1 and F-NS-10 at each temperature (Figure S12a) was further normalized by their area of F-(001) surface in Figure S12b. A similar *k_s* constant ($\text{h}^{-1}\cdot\text{g}\cdot\text{m}^{-2}$) can be obtained for these two samples at temperatures below 80 °C, confirming again that the area of F-(001) surface determines the activity for TiO₂ samples at low temperature. F-NS-10 provides a higher *k_s* constant above this temperature presumably due to its higher area of (101) surface. The activation energy (*E_a*) for TiO₂ samples was analyzed by Arrhenius plot (Figure 2e) and compared with their facet distribution in Figure 2f. As expected, F-NS-1 and F-NS-10 with different facet distribution show similar *E_a* around 60 kJ/mol while their F removed samples both exhibit 20 kJ/mol higher (i.e., 80 kJ/mol). This result further indicates that this reaction is facet-insensitive for pristine (101) and (001) surfaces and the ~20 kJ/mol difference in *E_a* can be exclusively attributed to the presence of F-(001) surface. This again explains why the area of F-(001) surface determines the activity for the as-prepared TiO₂ samples at temperature higher than 40 °C while not much difference in activity can be observed for F removed samples at all tested temperatures (Figure S8). Accordingly, we can conclude that the presence of F-(001) surface on a TiO₂ catalyst significantly lowers the *E_a* for this reaction and its area determines the observed activity.

It is believed that the electronic property (or Lewis acidity) of surface Ti atoms affects the adsorption/activation of *p*-NPP and hence the obtained activity. To gain more insight into the electronic effect imposed by fluorine to surface Ti atoms, TiO₂(001) slabs w/o surface F were firstly analyzed in Figure 3. Note that the relative electron density ($\Delta D_{\text{electron}}$) for each surface 5-coordinated Ti ($\text{Ti}_{5\text{C}}$) atom in this figure was obtained by comparing to their 6-coordinated counterpart in the bulk (i.e., $\Delta D_{\text{electron}} = D_{\text{electron}}(\text{Ti}_{5\text{C}}) - D_{\text{electron}}(\text{Ti}_{6\text{C}})$). For pristine (001) surface (Figure 3a), all $\text{Ti}_{5\text{C}}$ atoms exhibit similar $\Delta D_{\text{electron}}$ with a magnitude of 6.79×10^{-4} . Smaller magnitudes can be found for

Ti_{5C} atoms on F-(001) surface (Figure 3b), suggesting that the Ti_{5C} atoms on this surface are more acidic (i.e., electron deficient) than the pristine (001) surface. The F-attached Ti_{6C} indeed shows the lowest $\Delta D_{\text{electron}}$ among Ti atoms on F-(001) surface due to the formation of strong Ti-F bond (i.e., the only bond stronger than Ti-O). However, the F-attached Ti_{6C} should not directly participate in this reaction since it has no vacant orbital to interact with the coming *p*-NPP. Accordingly, the facilitated adsorption/activation of *p*-NPP observed over F-NS-1 and F-NS-10 should closely associate with those acidic Ti_{5C} atoms in a proximity to F on F-(001) surface.

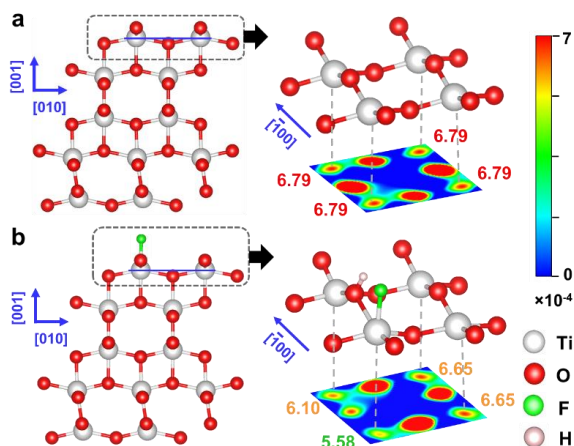


Figure 3. Side view and enlarged top view of the anatase TiO₂(001) slabs without (a) and with (b) surface fluorine (accompanied by an acidic proton). The relative electron density ($\Delta D_{\text{electron}}$) for each surface 5-coordinated Ti (Ti_{5C}) atom was obtained by comparing to their 6-coordinated counterpart in the bulk (i.e., $\Delta D_{\text{electron}} = D_{\text{electron}}(\text{Ti}_{5C}) - D_{\text{electron}}(\text{Ti}_{6C})$). The position of the slicing plane is blue highlighted. Note that the coverage of F (25%) used here does not represent the F coverage for both F-NS-1 and F-NS-10 samples (see below).

Conventional surface tools such as Ti_{2p} XPS (Figure 4a) and pyridine-infrared (Py-IR, Figure 4b) were adopted to unravel the nature of Ti_{5C} atoms predicted above on F-(001) surface. Although XPS has been widely adopted as a surface-sensitive tool to atom oxidation states, no shift of Ti_{2p} signal can be observed among TiO₂ samples w/o surface F (Figure 4a). From our point of view, the reactant molecule, *p*-NPP, interacts only with Ti_{5C} atoms on the topmost surface of TiO₂ samples. However, the sampling depth of XPS is depending on the penetration length of photoelectrons and hence it often averages signals > 10 atomic layers from the surface^[16], resulting a very similar XPS Ti_{2p} spectra among TiO₂ samples. Unfortunately, many reports simply draw a conclusion that no change in the electronic state of surface Ti atoms before/after F removal based on their XPS result^[15, 19, 20]. This may explain why different interpretations and even disagreement often found among researchers using F-capped TiO₂ as catalyst. On the other hand, pyridine, a Lewis base molecule, has been widely used with IR for acid sites characterization of catalysts. In general, the interaction between pyridine and surface Lewis acid (LA) sites generates two dominant IR signals at 1450 cm⁻¹ and 1600 cm⁻¹ with a minor IR signal at 1490 cm⁻¹ overlapped with surface Brønsted acid (BA) sites^[29]. As shown in Figure 4b, the presence of surface LA sites (i.e., Ti_{5C} atoms) for all TiO₂ samples can be confirmed by both dominant IR signals at 1448 cm⁻¹ and 1608 cm⁻¹. However, no shift in these two IR peaks can be observed

between TiO₂ samples w/o surface F because the pyridine is too basic to distinguish those Ti_{5C} atoms^[29]. The evolution of BA sites on the as-prepared TiO₂ samples (i.e., F-NS-1 and F-NS-10) with a strong IR signal at 1490 cm⁻¹ is due to the hydrogen bonding stabilization of protons by surface fluorine (Figure 4c) as evidenced by the decrease of this signal for F removed samples (i.e., NS-1 and NS-10, Figure 4b). Although the charge analysis in Figure 3 shows the strong electronic withdrawing effect imposed by surface F to Ti_{5C} atoms (i.e., the LA sites), many researchers may mistakenly attribute the enhanced activity to the surface F-induced BA sites since this is the only difference among TiO₂ samples they can observe using conventional surface techniques. However, a control experiment using conventional BA catalysts (i.e., HY zeolite) shows no enhance in activity compared to that of F-NS-1 (Figure S13).

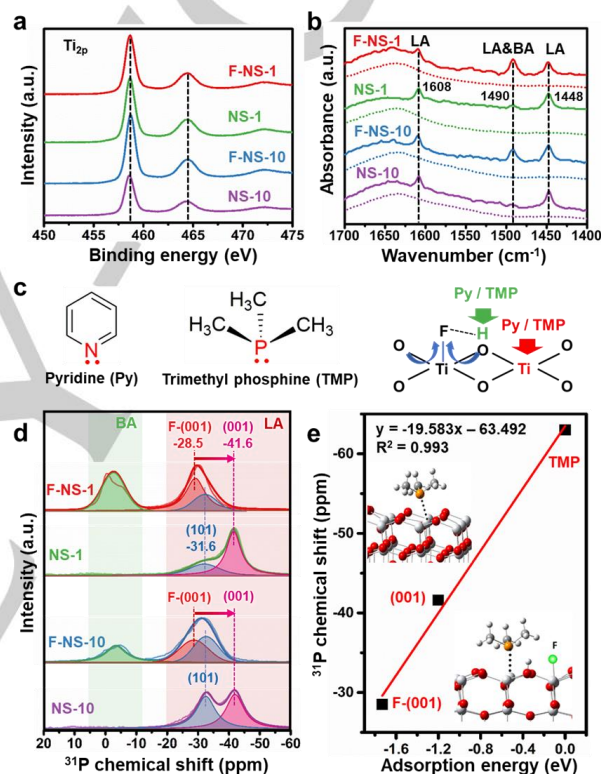


Figure 4. (a) Ti_{2p} XPS spectra of TiO₂ samples. (b) IR spectra of TiO₂ samples before (dash line) and after (solid line) pyridine adsorption. (c) Schematic illustration of the interaction between probe molecules (Py and TMP) with different acidic sites on TiO₂ surface. (d) TMP-assisted ³¹P NMR spectra of TiO₂ samples. (e) A correlation plot showing the linear relationship between the $\delta^{31}\text{P}$ of TMP-adsorbed TiO₂(001) facet w/o F and the corresponding calculated adsorption energy.

The use of ³¹P NMR with trimethylphosphine (TMP) as the probe molecule has been demonstrated by our group a promising method for the surface study of various metal oxides^[30-33]. In general, the ³¹P signal with chemical shift ($\delta^{31}\text{P}$) between 0 and -5 ppm can be attributed to the formation of TMPH⁺ species due to the surface BA site, while the coordination of TMP to a surface cation can generate $\delta^{31}\text{P}$ in a wider range from -20 to -60 ppm depending on its LA strength (or electron density)^[34]. Herein, the degree of this Lewis acid-base interaction (i.e., TMP \leftrightarrow Ti_{5C}) determines the electron density of ³¹P nuclei and hence the corresponding $\delta^{31}\text{P}$ in ³¹P NMR. A stronger TMP \rightarrow Ti_{5C} bond formation over Ti_{5C} with high

LA strength would thus push the $\delta^{31}\text{P}$ downfield (i.e., shift towards positive ppm). Figure 4d shows the $\text{TMP-}^{31}\text{P}$ NMR spectra of F-NS-1, F-NS-10 and their F removed samples. It is clear that $\text{TMP-}^{31}\text{P}$ NMR can provide more surface details compared with conventional XPS (Figure 4a) and IR (Figure 4b) since the peak shift and change in intensity are both distinguished among TiO_2 samples w/o surface F. For the BA range (i.e., $\delta^{31}\text{P}$ at 0 ~ -5 ppm), F-NS-1 with higher F-(001) surface area indeed shows a stronger signal than that of F-NS-10, while no BA signal in this range can be observed for their F removed samples (Figure 4d). This result again confirms above observation that (1) surface F can induce BA sites on F-(001) and (2) its removal by NaOH wash is very efficient with no BA sites left. Since the electronic state of surface $\text{Ti}_{5\text{C}}$ atoms is believed to vary with their host surfaces, one would expect to see two distinct ^{31}P signals in the LA range (i.e., $\delta^{31}\text{P}$ at -20 ~ -60 ppm) for each TiO_2 sample. For example, the NS-1 sample enclosed by 73.1%/26.9% of (001)/(101) surface shows a dominant $\delta^{31}\text{P}$ at -41.6 ppm and a minor $\delta^{31}\text{P}$ at -31.6 ppm (Figure 4d). These two $\delta^{31}\text{P}$ signals can be individually assigned to $\text{Ti}_{5\text{C}}$ atoms on pristine (001) and (101) surfaces. Considering that pristine (001) consists of 100% $\text{Ti}_{5\text{C}}$ while (101) provides only 50% $\text{Ti}_{5\text{C}}$ ^[15], this explains why NS-10 sample with 35.3%/64.7% of (001)/(101) surface displays similar intensity at both $\delta^{31}\text{P}$ (Figure 4d). Since F binds specifically to the (001) surface, the deconvoluted $\delta^{31}\text{P}$ at -28.5 ppm for F-NS-1 and F-NS-10 samples (Figure 4d, with a fixed $\delta^{31}\text{P}$ at -31.6 ppm) can be attributed to the remaining $\text{Ti}_{5\text{C}}$ atoms on F-(001) surface with F- $\text{Ti}_{6\text{C}}$ species nearby. The 13 ppm downshift for $\text{Ti}_{5\text{C}}$ atoms from -41.6 ppm of pristine (001) to -28.5 ppm of F-(001) confirms the electron withdrawing effect imposed by surface F to surrounding $\text{Ti}_{5\text{C}}$ atoms as suggested in Figure 3. Since the adsorption energy (E_{ad}) of TMP on a given facet is believed to be proportional to its corresponding $\delta^{31}\text{P}$, the E_{ad} of TMP was further calculated as -1.73 eV for F-(001) and -1.2 eV for pristine (001) (Figure S14), which indeed displays a good linear relationship with the experimental $\delta^{31}\text{P}$ value (Figure 4e). Although F-NS-1 has a doubled area of F-(001) surface (cf. F-NS-10, Table S1), similar F coverage (~40%) was obtained for both shapes as expected (see SI for detailed calculation).

Since the adsorption (step 1) and activation (step 2) of reactants on catalysts' surface are both critical steps in heterogeneous catalysis, the surface information revealed by $\text{TMP-}^{31}\text{P}$ NMR can further provide insights into the interplay between TiO_2 samples and *p*-NPP. F-NS-1 and NS-1 with same morphology, surface area and the (001)/(101) ratio (Table S1) were thus picked for an in-depth comparison. The facilitated adsorption of *p*-NPP on F-(001) surface was visualized by scanning TEM-electron energy loss spectroscopy (STEM-EELS). As shown in Figure 5a, F-NS-1 displays a strong phosphorus signal from surface adsorbed *p*-NPP while this signal is very weak for NS-1 with pristine (001) surface. The considerable difference in *p*-NPP adsorption also reflects to their IR (Figure 5b) and Raman (Figure S15) spectra. Both IR and Raman fingerprint of *p*-NPP (black line) can be identified on F-NS-1 (red line) while not for NS-1 (green line) after *p*-NPP adsorption. The upshift of P=O vibration frequency from 1098 cm^{-1} to 1122 cm^{-1} (Figure 5b) further suggests the subsequent *p*-NPP activation on F-(001) surface. Since the rest phosphoryl oxygens of *p*-NPP can interact with up to two surface cations at the same time, this allows surface-adsorbed *p*-NPP being

activated either synergistically by a BA (i.e., acidic proton) and a LA site (i.e., $\text{Ti}_{5\text{C}}$) or by two BA/LA sites.

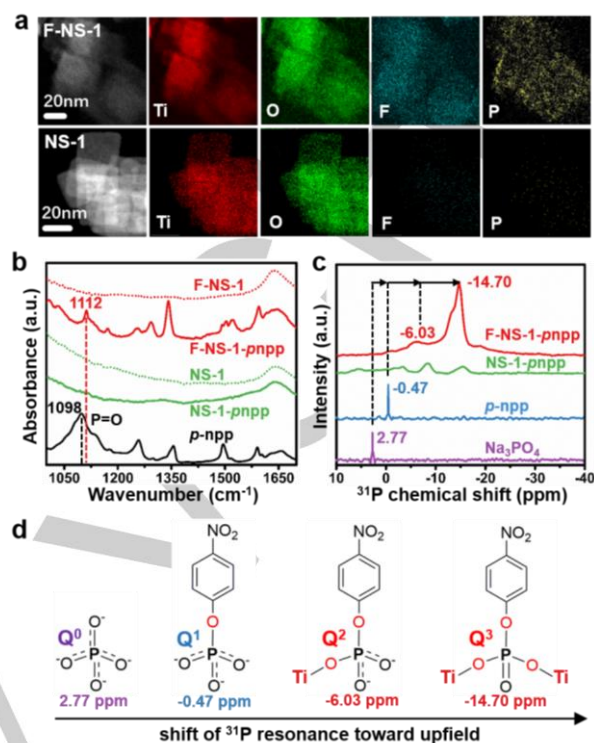
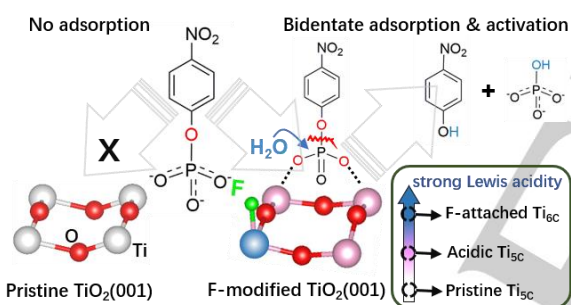


Figure 5. (a) TEM-EELS Ti/O/F/P mapping of *p*-NPP adsorbed F-NS-1 and NS-1 samples. (b) IR spectra of F-NS-1 and NS-1 samples before (dash line) and after (solid line) *p*-NPP adsorption. (c) ^{31}P NMR spectra of *p*-NPP adsorbed F-NS-1 and NS-1 samples (the spectra of Na_3PO_4 and *p*-NPP solution were included for comparison). (d) The relationship between ^{31}P chemical shift and the configuration of phosphate group with various chemical environments.

^{31}P NMR was further adopted to investigate the atomic configuration of adsorbed *p*-NPP on F-(001) surface. As shown in Figure 5c, the *p*-NPP adsorbed F-NS-1 shows a dominant $\delta^{31}\text{P}$ signal at -14.70 ppm and a minor one at -6.03 ppm, while no apparent signals at these two positions can be observed for NS-1. This result is in line with STEM-EELS (Figure 5a), IR (Figure 5b) and Raman (Figure S15) studies above suggesting the facilitated adsorption of *p*-NPP on F-NS-1. To evaluate the electronic effect of BA (or acidic proton) to *p*-NPP phosphorus, the ^{31}P NMR spectra of phosphate compounds with different degree of protonation was firstly recorded (Figure S16). A continuous upshift of $\delta^{31}\text{P}$ can be observed with the increased degree of protonation from PO_4^{3-} (Q⁰, 2.77 ppm), HPO_4^{2-} (Q¹, 2.59 ppm), H_2PO_4^- (Q², 0.18 ppm) to H_3PO_4 (Q³, 0 ppm). Note that the "i" of Qⁱ represents the number of bridged oxygens in a given phosphate compound. Each P-O→H bond formation disturbs the electron structure of center phosphorus, making it electron rich with an upshifted $\delta^{31}\text{P}$. Since the sequential protonation of PO_4^{3-} only shifts the $\delta^{31}\text{P}$ towards upfield within 3 ppm (Figure S16), this cannot explain the considerable shift of $\delta^{31}\text{P}$ from -0.47 ppm of *p*-NPP (Q¹) to -6.03 ppm and -14.70 ppm (Figure 5c). The possibility of the activation of *p*-NPP by BA sites alone on F-(001) is therefore eliminated. This also explains why HY zeolite is inactive at 60 °C (Figure S13). In stark contrast, a considerable shift in $\delta^{31}\text{P}$ has been reported when the oxygen atoms of PO_4^{3-} is bonded with transition metal cations^[35, 36]. The

phosphorus of PO_4^{3-} also becomes more and more shielded with increasing number of surrounding cations. For example, Knowles et al. incorporated TiO_2 into the P_2O_5 -based glass samples and found the formation of each P-O→Ti bond shifts the $\delta^{31}\text{P}$ to upfield about 7 ppm^[36]. Accordingly, the $\delta^{31}\text{P}$ of the adsorbed *p*-NPP at -6.03 ppm and -14.70 ppm (Figure 5c) can be attributed to the formation of Q^2 (monodentate) and Q^3 (bidentate) configurations on F-(001) surface (Figure 5d). The dominant $\delta^{31}\text{P}$ signal at -14.70 ppm also suggests that *p*-NPP preferentially adsorbs on this surface with Q^3 configuration, which weakens the phosphate ester bond for subsequent dephosphorylation. We can thus conclude that the strong Lewis acidity of $\text{Ti}_{5\text{C}}$ atoms on F-(001) surface not only promotes the adsorption of *p*-NPP, the formation of Q^3 configuration on this surface further lowers the E_a for its subsequent activation. The E_{ad} of *p*-NPP with bidentate configuration on both surfaces was also calculated (Figure S19). However, the result cannot explain the considerable difference in the amount of surface *p*-NPP observed between these two surfaces (Figure 5a-c and Figure S15), presumably due to the involvement of solvent (see SI for detailed discussion). Scheme 2 shows the proposed mechanism for *p*-NPP adsorption/activation over $\text{TiO}_2(001)$ w/o surface F. Most importantly, the activity of F-NS-1 was found even comparable to CeO_2 cube at 60 °C (Figure S13 and Figure S17). See SI for a more detailed discussion on the activity comparison with various CeO_2 surfaces in literature (Figure S18 and Table S3).



Scheme 2. Proposed mechanism for *p*-NPP dephosphorylation over $\text{TiO}_2(001)$ w/o surface F.

Since the first report by Yang et al. in 2008^[18], anatase TiO_2 with high coverage of F-capped (001) surface has been adopted in many literatures for a wide range of catalytic reactions^[15,18-20]. The surface pre-adsorbed fluorine (i.e., surfactant) is often removed by either calcination or NaOH wash before catalytic testing. Many literatures (even for those published in high-impact journals) simply concluded no change in the electronic state of surface Ti atoms after F removal based on XPS results^[15,18-20]. However, for commercial XPS equipped with Al as X-ray source (1486.6 eV), $\text{Ti}_{2\text{p}}$ photoelectrons with energy about 1000 eV can penetrate few nanometers from TiO_2 surface and hence provide an averaged oxidation state of Ti cations. Since the thickness of F-NS-1 sample is 4.89 nm, commercial XPS is undoubtedly a bulk technique for not only TiO_2 samples here (Figure S2) but also many nanocatalysts used in literatures. Given that heterogeneous catalysis mainly involves active sites on the topmost surface of the catalyst, those structure-activity correlations established in literatures based on XPS are thus questionable. Some researchers may realize the importance of obtaining the electronic state of active sites as this property can significantly affect the adsorption/activation of

reactants and hence the obtained activity. However, conventional probe-assisted IR provides very limited information^[29] for both catalyst' surface (Py-IR, Figure 4b) and its interplay with the reactant molecules (e.g., *p*-NPP, Figure 5b). Taking *p*-NPP dephosphorylation over TiO_2 as an example here, we strongly suggest the adoption of advanced surface characterizations such as probe-assisted NMR to ensure a solid structure-activity correlation is unambiguously built.

Conclusion

In summary, we demonstrate that TiO_2 with F-modified (001) surface can activate *p*-NPP dephosphorylation at nearly room temperature. As predicted by model analysis, the electronic withdrawing effect of fluorine imposed on $\text{TiO}_2(001)$ surface strongly manipulates the electronic state of surrounding $\text{Ti}_{5\text{C}}$ atoms by making them very acidic with 13 ppm shift in $\text{Ti}_{5\text{C}}^{31}\text{P}$ NMR. Those acidic $\text{Ti}_{5\text{C}}$ atoms on F-(001) surface were found to facilitate the bidentate adsorption of *p*-NPP and its later activation with an E_a of 60 kJ/mol, which is ~20 kJ/mol lower than that of pristine (001) and (101) surfaces. The as-prepared TiO_2 samples with F-(001) surface can thus activate this reaction at temperature as low as 40 °C (cf. F removed counterparts at > 80 °C). This also explains why the F-NS-1 sample with doubled area of F-(001) surface provides *k* constant nearly two times higher than that of F-NS-10. Our study highlights the importance of unraveling the electronic effect imposed by surface pre-adsorbed species (e.g., surfactant) as it can significantly affect the physicochemical properties of active sites on catalysts' surface and hence the observed activity. The successful implementation of this will not only resolve the disagreement found among literatures but also provide a solid guideline for the design (or seeking) of catalysts with high activity.

Acknowledgements

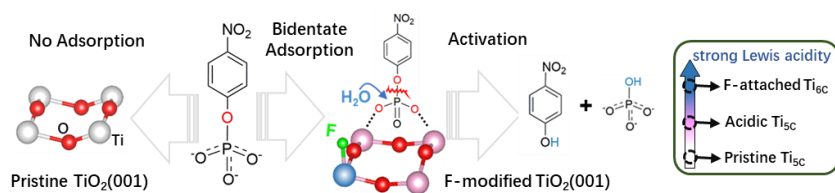
We thank National Natural Science Foundation of China (21902138, 21802164, 22032005 and U1832148), the Hong Kong Research Grants Council (CityU 21301719 and CityU 11300020) for funding support. The authors acknowledge Dr. Jin Shang for the BET measurement.

Keywords: Electronic state manipulation • Dephosphorylation • Titanium dioxide • Surface characterization • Nuclear magnetic resonance

- [1] N. N. Greenwood, A. Earnshaw, *Chemistry of the Elements*. **2012**.
- [2] J. Ali, D. C. Sharma, A. Bano, A. Gupta, S. Sharma, P. Bajpai, N. Pathak, *Enzymes in Food Biotechnology* **2019**, 503-519.
- [3] D. Cordell, S. White, *Sustainability* **2011**, 3, 2027-2049.
- [4] D. Cordell, J.-O. Drangert, S. White, *Glob. Environ. Change* **2009**, 19, 292-305.
- [5] F. Tan, Y. Zhang, J. Wang, J. Wei, Y. Cai, X. Qian, *J. Mass Spectrom* **2008**, 43, 628-32.
- [6] M. H. Kuchma, C. B. Komanski, J. Colon, A. Teblum, A. E. Masunov, B. Alvarado, S. Babu, S. Seal, J. Summy, C. H. Baker, *Nanomedicine* **2010**, 6, 738-44.
- [7] A. A. Vernekar, T. Das, G. Muges, *Angew. Chem. Int. Ed.* **2016**, 55, 1412-1416.
- [8] M. J. Manto, P. Xie, C. Wang, *ACS Catal.* **2017**, 7, 1931-1938.
- [9] G. C. Shearer, J. G. Vitillo, S. Bordiga, S. Svelle, U. Olsbye, K. P. Lillerud, *Chem. Mater.* **2016**, 28, 7190-7193.

- [10] K. Khulbe, P. Roy, A. Radhakrishnan, G. Mugesh, *ChemCatChem* **2018**, *10*, 4826-4831.
- [11] K. Khulbe, G. Mugesh, *Polyhedron* **2019**, *172*, 198-204.
- [12] J. Yang, K. Li, C. Li, J. Gu, *Angew. Chem. Int. Ed.* **2020**, *59*, 22952–22956.
- [13] Z. Tan, T.-S. Wu, Y.-L. Soo, Y.-K. Peng, *Appl. Catal. B.* **2020**, *264*, 118508.
- [14] U. G. Survey, MINERAL COMMODITY SUMMARIES 2020. **2020**, 137.
- [15] G. Liu, H. G. Yang, J. Pan, Y. Q. Yang, G. Q. Lu, H. M. Cheng, *Chem. Rev.* **2014**, *114*, 9559-9612.
- [16] Y.-K. Peng, S. C. E. Tsang, *Nano Today* **2018**, *18*, 15-34.
- [17] M. A. Boles, D. Ling, T. Hyeon, D. V. Talapin, *Nat. Mater.* **2016**, *15*, 141-153.
- [18] H. G. Yang, C. H. Sun, S. Z. Qiao, J. Zou, G. Liu, S. C. Smith, H. M. Cheng, G. Q. Lu, *Nature* **2008**, *453*, 638-41.
- [19] S. Liu, J. Yu, M. Jaroniec, *Chem. Mater.* **2011**, *23*, 4085-4093.
- [20] W. Q. Fang, X.-Q. Gong, H. G. Yang, *J. Phys. Chem. Lett.* **2011**, *2*, 725-734.
- [21] H. G. Yang, G. Liu, S. Z. Qiao, C. H. Sun, Y. G. Jin, S. C. Smith, J. Zou, H. M. Cheng, G. Q. Lu, *J Am Chem Soc* **2009**, *131*, 4078–4083.
- [22] C. Z. Wen, J. Z. Zhou, H. B. Jiang, Q. H. Hu, S. Z. Qiao, H. G. Yang, *Chem. Commun.* **2011**, *47*, 4400-4402.
- [23] M. Li, Y. Chen, W. Li, X. Li, H. Tian, X. Wei, Z. Ren, G. Han, *Small* **2017**, *13*, 1604115.
- [24] L. Ruan, X. Wang, T. Wang, Z. Ren, Y. Chen, R. Zhao, D. Zhou, G. Fu, S. Li, L. Gao, Y. Lu, Z. Wang, H. Tian, X. Kong, G. Han, *ACS Appl. Mater. Interfaces* **2019**, *11*, 37256-37262.
- [25] U. Diebold, *Surf. Sci. Rep.* **2003**, *48*, 53–229.
- [26] A. S. Barnard, L. A. Curtiss, *Nano Lett.* **2005**, *5*, 1261-1266
- [27] X. Han, Q. Kuang, M. Jin, Z. Xie, L. Zheng, *J. Am. Chem. Soc.* **2009**, *131*, 3152-3153.
- [28] Y. K. Peng, Y. Hu, H. L. Chou, Y. Fu, I. F. Teixeira, L. Zhang, H. He, S. C. E. Tsang, *Nat. Commun.* **2017**, *8*, 675.
- [29] A. Zheng, S. B. Liu, F. Deng, *Chem Rev* **2017**, *117*, 12475-12531.
- [30] Y. K. Peng, L. Ye, J. Qu, L. Zhang, Y. Fu, I. F. Teixeira, I. J. McPherson, H. He, S. C. E. Tsang, *J. Am. Chem. Soc.* **2016**, *138*, 2225-34.
- [31] Y. K. Peng, H. L. Chou, S. C. E. Tsang, *Chem. Sci.* **2018**, *9*, 2493-2500.
- [32] Y. K. Peng, B. Keeling, Y. Li, J. Zheng, T. Chen, H. L. Chou, T. J. Puchler, R. A. Taylor, S. C. E. Tsang, *Chem. Commun.* **2019**, *55*, 4415-4418.
- [33] Z. Tan, G. Li, H.-L. Chou, Y. Li, X. Yi, A. H. Mahadi, A. Zheng, S. C. E. Tsang, Y.-K. Peng, *ACS Catal.* **2020**, *10*, 4003-4011.
- [34] X. Yi, H. H. Ko, F. Deng, S. B. Liu, A. Zheng, *Nat Protoc* **2020**, *15*, 3527- 3555.
- [35] A. Kiani, L. S. Cahill, E. A. Abou Neel, J. V. Hanna, M. E. Smith, J. C. Knowles, *Mater. Chem. Phys.* **2010**, *120*, 68-74.
- [36] A. Kiani, J. V. Hanna, S. P. King, G. J. Rees, M. E. Smith, N. Roohpour, V. Salih, J. C. Knowles, *Acta Biomater.* **2012**, *8*, 333-340.

Entry for the Table of Contents



We demonstrate that TiO₂ with F-modified (001) surface can activate *p*-NPP dephosphorylation for the first time at nearly room temperature. The electronic withdrawing effect of fluorine imposed on TiO₂(001) surface strongly manipulates the electronic state of surrounding Ti_{5c} atoms by making them very acidic, facilitating not only the bidentate adsorption of *p*-NPP but also its subsequent activation.